



# Chemical characterisation of water-soluble ions in atmospheric particulate matter on the east coast of Peninsular Malaysia

Naomi J. Farren<sup>1</sup>, Rachel E. Dunmore<sup>1</sup>, Mohammed Iqbal Mead<sup>2</sup>, Mohd Shahrul Mohd Nadzir<sup>3,4</sup>, Azizan Abu Samah<sup>5</sup>, Siew-Moi Phang<sup>5</sup>, Brian J. Bandy<sup>6</sup>, William T. Sturges<sup>6</sup>, and Jacqueline F. Hamilton<sup>1</sup>

<sup>1</sup>Wolfson Atmospheric Chemistry Laboratories, Department of Chemistry, University of York, York, YO10 5DD, UK

<sup>2</sup>Centre for Atmospheric Informatics and Emissions Technology, School of Energy, Environment and Agrifood/Environmental Technology, Cranfield University, Cranfield, UK

<sup>3</sup>Centre for Tropical Climate Change System (IKLIM), Institute of Climate Change, Universiti Kebangsaan Malaysia, 43600 Bangi, Selangor, Malaysia

<sup>4</sup>School of Environmental Science and Natural Resources, Faculty of Science and Technology, Universiti Kebangsaan Malaysia, 43600 Bangi, Selangor Darul Ehsan, Malaysia

<sup>5</sup>Institute of Ocean and Earth Sciences, University of Malaya, Kuala Lumpur, Malaysia

<sup>6</sup>Centre for Ocean and Atmospheric Sciences, School of Environmental Sciences, University of East Anglia, Norwich, UK

**Correspondence:** Jacqueline F. Hamilton (jacqui.hamilton@york.ac.uk)

Received: 6 February 2018 – Discussion started: 24 April 2018

Revised: 13 January 2019 – Accepted: 18 January 2019 – Published: 6 February 2019

**Abstract.** Air quality on the east coast of Peninsular Malaysia is influenced by local anthropogenic and biogenic emissions as well as marine air masses from the South China Sea and aged emissions transported from highly polluted East Asian regions during the winter monsoon season. An atmospheric observation tower has been constructed on this coastline at the Bachok Marine Research Station. Daily PM<sub>2.5</sub> samples were collected from the top of the observation tower over a 3-week period, and ion chromatography was used to make time-resolved measurements of major atmospheric ions present in aerosol. SO<sub>4</sub><sup>2-</sup> was found to be the most dominant ion present and on average made up 66% of the total ion content. Predictions of aerosol pH were made using the ISORROPIA II thermodynamic model, and it was estimated that the aerosol was highly acidic, with pH values ranging from -0.97 to 1.12. A clear difference in aerosol composition was found between continental air masses originating from industrialised regions of East Asia and marine air masses predominantly influenced by the South China Sea. For example, elevated SO<sub>4</sub><sup>2-</sup> concentrations and increased Cl<sup>-</sup> depletion were observed when continental air masses that had passed over highly industrialised regions of East Asia arrived at the measurement site. Correlation analyses of the ionic species and assessment of ratios between different

ions provided an insight into common sources and formation pathways of key atmospheric ions, such as SO<sub>4</sub><sup>2-</sup>, NH<sub>4</sub><sup>+</sup> and C<sub>2</sub>O<sub>4</sub><sup>2-</sup>. To our knowledge, time-resolved measurements of water-soluble ions in PM<sub>2.5</sub> are virtually non-existent in rural locations on the east coast of Peninsular Malaysia. Overall this dataset contributes towards a better understanding of atmospheric composition in the Maritime Continent, a region of the tropics that is vulnerable to the effects of poor air quality, largely as a result of rapid industrialisation in East Asia.

## 1 Introduction

The tropical Maritime Continent, a region in Southeast Asia between 10° S–20° N and 90–150° E, is a complex distribution of islands and peninsulas and incorporates countries such as Malaysia, Indonesia, the Philippines and Papua New Guinea (Neale and Slingo, 2003). It lies within a tropical warm pool that extends eastwards from the Indian Ocean to the Western Pacific and is home to some of the warmest ocean temperatures in the world. Tropical regions such as the Maritime Continent are of central importance for the chemistry–climate system (Carpenter et al., 2010). For example, high photochemical activity in these regions means

that global atmospheric lifetimes of key atmospheric species, such as methane and ozone, are controlled by destruction rates in the tropics (Lawrence et al., 2001; Bloss et al., 2005). In terms of ocean productivity, the observed decrease in primary productivity in low-latitude oceans has been linked to a reduced availability of nutrients for phytoplankton growth, caused by changes in upper-ocean temperature and stratification (Behrenfeld et al., 2006). Furthermore, the wind circulation system in the Maritime Continent is influenced by seasonal Asian monsoons, which are controlled by the natural oscillation of the intertropical convergence zone (ITCZ). During the Northern Hemisphere winter, a large anticyclone forms over Siberia each year, creating strong northeasterly monsoon winds in the South China Sea (northeast monsoon). These strong northeasterlies can transport air masses from rapidly developing East Asian countries (e.g. China, Japan, Vietnam, and North and South Korea) across the South China Sea to the Maritime Continent (Zhang et al., 1997; Garreaud, 2001; Oram et al., 2017). In addition, cold-surge events occur regularly throughout the winter monsoon season and last several days. Cold surges occur as a result of a southeasterly movement of the anticyclone and are characterised by cold air masses over Southern China and strengthening of the northeasterly monsoon winds in the South China Sea (Zhang et al., 1997). The transport of pollution from East Asia to the tropics during the monsoon season, particularly during cold surges, means that rural areas such as the east coast of Peninsular Malaysia are potentially at an elevated risk of the detrimental effects of poor air quality.

Tropical regions are highly important for atmospheric research, and whilst long-term atmospheric observations exist (Robinson et al., 2014; Pyle et al., 2011), there are fewer measurements than in the mid and high latitudes. The Bachok Marine Research Station (lat 6.00892, long. 102.42504) has been set up on the east coast of Peninsular Malaysia and is ideally located for studying the outflow of these highly industrialised regions and for investigating the interaction with cleaner air in the Southern Hemisphere. The research station, located approximately 30 km away from Kota Bharu, forms part of the Institute of Ocean and Earth Sciences at the University of Malaya (UM). An atmospheric observation tower facing the South China Sea has been constructed at the research station; this has been built for the specific purpose of monitoring long-range transported pollution, air-sea exchange and coastal meteorology. The research station is working towards designation as a regional Global Atmospheric Watch (GAW) centre, which will be a valuable addition to the network of other global and regional GAW sites in the Maritime Continent, as shown in Fig. 1 (GAW-SIS, 2017).

In January and February 2014, an instrument demonstration campaign was carried out to assess the capabilities of the new research station. This was funded by the Natural Environment Research Council (NERC) and UM and involved several UK universities, as well as the National Cen-

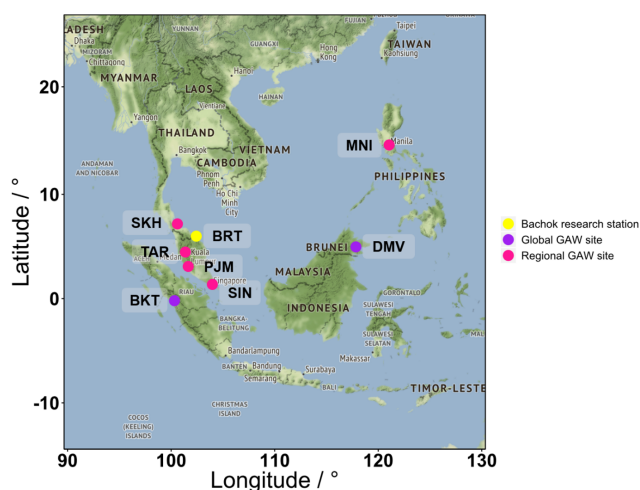


**Figure 1.** Location of the Bachok research station (BRT) and the global and regional GAW sites in the Maritime Continent: Danum Valley in Malaysia (DMV), Bukit Kototabang in Indonesia (BKT), Manila in Philippines (MNI), Songkhla in Thailand (SKH), Tanah Rata in Malaysia (TAR), Petaling Jaya in Malaysia (PJM) and Singapore (SIN) (GAW-SIS, 2017).

tre for Atmospheric Science (NCAS), UM and the Malaysian Meteorological Department (MMD). As part of this study, Dunmore et al. (2016) used a specialised multidimensional gas chromatography technique to accurately measure atmospheric mixing ratios of C<sub>5</sub>–C<sub>13</sub> volatile organic compounds (VOCs) with a wide range of functionalities. Furthermore, Dominick et al. (2015) characterised the particulate matter in Bachok by studying the influence of northeasterly winds on the patterns of particle mass and particle number concentration size distributions. Both studies highlighted the fact that the site is influenced by a mixture of local anthropogenic and biogenic emissions, clean marine air masses, and aged emissions transported from East Asia.

To extend upon these studies, it is important to investigate atmospheric aerosol composition in the Bachok region. A better understanding of aerosol chemical composition is essential as aerosols play an important role in atmospheric processes and climate change. For example, aerosols can modify the global radiation budget both directly, by scattering and absorbing solar radiation, and indirectly, by altering cloud properties and lifetime (Charlson et al., 1991). The strength of these direct and indirect effects depends partly on the particle concentration and size distribution, but also on the chemical composition.

There are a limited number of studies that focus on particulate matter composition on the east coast of Peninsular Malaysia, and to our knowledge the composition of ionic species has not been determined at any rural locations along this coastline. For example, Tahir et al. (2013) studied the composition of major elements and water-soluble ionic species in PM<sub>2.5</sub> and PM<sub>10</sub> samples on the east coast of

Peninsular Malaysia, but the samples were collected at an urban coastal city, Kuala Terengganu. This study used principal component analysis to determine the main sources of both fine and coarse particles, which were found to be soil dust, marine aerosol, vehicle exhaust, secondary aerosol, road dust and biomass burning. In addition, Ismail et al. (2016) studied PM<sub>10</sub> concentrations in three major cities (Kota Bharu, Kuala Terengganu and Kuantan) on the east coast of Peninsular Malaysia between 2006 and 2012. The study showed that during the northeast monsoon, the air arriving at the sites had originated from China and the Philippines and travelled over the South China Sea. During the southwest monsoon, the air came from Indonesia via the Strait of Malacca. Over the 6-year period, it was found that the atmospheric PM<sub>10</sub> mass was directly proportional to the rate of urbanisation in each of the three cities.

In this study, measurements of water-soluble ions in atmospheric aerosol at a rural coastal location on the east coast of Peninsular Malaysia are presented. Analysis of temporal variation of different ionic species has been carried out and backward air mass trajectories have been used to determine the influence of air mass origin on aerosol composition. Correlation analyses of the ionic species and assessment of ratios between different ions have provided an insight into common sources and formation pathways of key atmospheric ions. This study contributes towards a better understanding of atmospheric composition in the rural Bachok region, which is vulnerable to the effects of poor air quality, largely as a result of rapid industrialisation in East Asia.

## 2 Experiment

### 2.1 Sample collection and extraction

Thirty PM<sub>2.5</sub> samples were collected at the Bachok Marine Research Station (lat 6.00892, long. 102.42504) between 18 January and 7 February 2014. The samples were collected at the top of an atmospheric observation tower (18 m height) using a high-volume air sampler (Ecotech HiVol 3000, Victoria, Australia) operating at 1.13 m<sup>3</sup> min<sup>-1</sup> over 24 h sampling intervals. The tower is located on the coastline of the South China Sea and is within 100 m of the shore. A 3-day intensive measurement period was in operation between midday (local time) on 30 January 2014 and midday on 2 February 2014, in which filters were collected every 4–8 h. The quartz fibre filters (20.3 cm × 25.4 cm) supplied by Whatman (Maidstone, UK) were pre-baked at 550 °C for a minimum of 12 h prior to sample collection. After sample collection, the filters were wrapped in aluminium foil and stored at -18 °C until analysis. To prepare the samples for analysis, 5.7 cm<sup>2</sup> of each sample was dissolved in 2 mL Milli-Q water and sonicated for 30 min at room temperature. The extract was filtered using a Millex-GP 33 mm diameter hydrophilic syringe filter

with a pore size of 0.22 µm (Millipore UK Limited, Watford, UK) and made up to a final volume of 2.5 mL.

### 2.2 Eluents and analytical standards

Ultrapure Milli-Q water (18 MΩ cm<sup>-1</sup>) from an ELGA Lab-Water purification system was used to prepare all the required eluents and analytical standards. A 20 mM solution of methanesulfonic acid was used as the eluent for cation exchange chromatography, and for anion exchange chromatography, a solution of 8 mM Na<sub>2</sub>CO<sub>3</sub> / 1 mM NaHCO<sub>3</sub> was prepared. Using a variety of salts and organic acids, individual analytical standards containing 500 ppm of each target ion (Cl<sup>-</sup>, NO<sub>2</sub><sup>-</sup>, NO<sub>3</sub><sup>-</sup>, PO<sub>4</sub><sup>3-</sup>, SO<sub>4</sub><sup>2-</sup>, CH<sub>3</sub>SO<sub>3</sub><sup>-</sup>, C<sub>2</sub>O<sub>4</sub><sup>2-</sup>, Na<sup>+</sup>, NH<sub>4</sub><sup>+</sup>, K<sup>+</sup>, Mg<sup>2+</sup> and Ca<sup>2+</sup>) were prepared in Milli-Q water. The salts and organic acids were purchased from either Sigma-Aldrich Ltd. (Dorset, UK) or Fisher Scientific Ltd. (Loughborough, UK).

### 2.3 Chromatographic analysis

Chromatographic analysis was carried out using a Thermo Scientific Dionex ICS-1100 ion chromatography system equipped with an AS-DV autosampler. The column configuration used for anion exchange consisted of an IonPac AG14A guard column (4 mm × 50 mm) and an IonPac AS14A analytical column (4 mm × 250 mm). Cation exchange chromatography was performed using an IonPac CG12A guard column (4 mm × 50 mm) and an IonPac CS12A analytical column (4 mm × 250 mm). ASRS 300 and CSRS 300 self-regenerating suppressors (4 mm) were used for anion and cation exchange respectively. All columns and suppressors were supplied from Thermo Scientific Dionex. The run times for the anion and cation separations were 18 and 15 min respectively. The suppressor current was 45 mA for anion exchange mode and 59 mA for cation exchange mode. For all separations, the instrument was operated in isocratic mode at a flow rate of 1 mL min<sup>-1</sup> and a column oven temperature of 30 °C. The injection volume was 100 µL and the data collection rate was 5 Hz. The system relied on a DS6 heated conductivity cell for ion detection, and all data were analysed using Thermo Scientific Chromeleon 7.1 Chromatography Data System software.

### 2.4 Method validation

Using isocratic elution methods for both cation and anion exchange chromatography, the target ions were successfully separated. Recovery tests were performed by spiking 5.7 cm<sup>2</sup> of quartz fibre filters (Whatman, Maidstone, UK) with 1 µg of each target ion (20 µL of a 50 ppm mixed ion solution). Prior to spiking, the filters were pre-baked at 550 °C for 6 h and wrapped in aluminium foil and stored at -18 °C until required. The spiked filters were dissolved in 2 mL of Milli-Q water and sonicated for 30 min at room temperature. The extract was filtered using a Millex-GP 33 mm diameter hy-

drophilic syringe filter with a pore size of 0.22  $\mu\text{m}$  (Millipore UK Limited, Watford, UK) and made up to a final volume of 2.5 mL. The recovery of the target ions from the filter papers ranged from 74.5 % to 98.2 % for the target anions, and 78.3 % to 87.3 % for the target cations, with the exception of  $\text{Ca}^{2+}$  for which a recovery level of 123.3 % was calculated. Recovery tests were carried out in triplicate, and  $\% \text{RSD}_{\text{rec}}$  remained below 8 % for all the ions. The recovery of  $\text{Ca}^{2+}$  should not have exceeded 100 %, and the result may be attributed to inconsistencies in the amount of  $\text{Ca}^{2+}$  present on the blank filter, or due to  $\text{Ca}^{2+}$  contamination during sample collection or storage. A 100 % recovery was assumed for  $\text{Ca}^{2+}$  during the data analysis process. Further details of the individual recovery levels and associated errors can be found in the Supplement (Table S1). Procedural blanks were also carried out using quartz fibre filters (5.7  $\text{cm}^2$ ), and blank subtractions were applied to any target ions found in detectable amounts. The blank peak areas for each ion and average blank contribution to field samples over the entire sampling period are provided in the Supplement, Table S1. The main instrumental parameters of the IC system were evaluated and are also detailed in the Supplement (Table S2). Instrumental limits of detection (LODs) and limits of quantification (LOQs) were calculated according to the EPA protocol 40 CFR 136; multiplying the standard deviation ( $N = 10$ , 5 ng for cations, 25 ng for anions) by the  $t$  value ( $N = 10$ , 95 % confidence interval) gave the LOD, and multiplying the standard deviation by 10 gave the LOQ (EPA, 2017; Ripp, 1996). For anion exchange chromatography, LODs and LOQs were in the range 5.5–21.0 ng and 25.3–144.2 ng respectively. For cation exchange chromatography, the LODs ranged from 0.5 to 2.1 ng and the LOQs ranged from 2.5 to 6.1 ng. On average, the instrument precision ( $\% \text{RSD}_{\text{ins}}$ ,  $n = 10$ ) was 4.2 % for the target cations and 12.8 % for the target anions. Total errors were estimated by combining errors with the instrument and the recovery process and remained below 15.4 % for all ions except  $\text{NO}_3^-$  (22.6 %).

## 2.5 Additional measurements

Individual VOCs were measured using a combined heart-cut and comprehensive two-dimensional gas chromatography system (GC – GC  $\times$  GC); a detailed description of the instrument design is provided in a separate study (Dunmore et al., 2016). Measurements of NO and  $\text{NO}_2$  were performed using a two channel 42i-TL commercial gas analyser (Thermo Scientific, MA, USA), and  $\text{SO}_2$  measurements were made using a Thermo Scientific 43i  $\text{SO}_2$  analyser. Meteorological data from the nearest meteorological station, the Sultan Ismail Petra Airport (lat 6.17208, long. 102.29288), were accessed from the Integrated Surface Database (NOAA, 2003). Hourly measurements of wind direction, wind speed, air temperature, dew point, atmospheric pressure and relative humidity were obtained. The 10-day backward air mass trajectories arriving at the sampling site were run every 3 h

throughout the entire measurement period. A receptor height of 10 m was chosen to represent the measurements made on the sampling tower. The trajectories were computed using the Hybrid Single-Particle Lagrangian Integrated Trajectory (HYSPLIT) model (Stein et al., 2015; Draxler, 1999; Draxler and Hess, 1998, 1997), and the data were analysed using the openair package in RStudio (Carslaw and Ropkins, 2012; Carslaw, 2015).

## 2.6 ISORROPIA II model

Predictions of aerosol pH were made using the ISORROPIA-II thermodynamic equilibrium model. Although these models produce better results when gas phase measurements such as  $\text{NH}_3$  and  $\text{HNO}_3$  are available, it is possible to use the ion measurements obtained in this study to make a prediction of aerosol pH (Fountoukis and Nenes, 2007). Calculations were made in reverse mode, in which known quantities are temperature, relative humidity, and particle phase concentrations of  $\text{NH}_4^+$ ,  $\text{SO}_4^{2-}$ ,  $\text{Na}^+$ ,  $\text{Cl}^-$ ,  $\text{NO}_3^-$ ,  $\text{Ca}^{2+}$ ,  $\text{K}^+$  and  $\text{Mg}^{2+}$ . ISORROPIA II assumes that the particles are internally mixed; this is a reasonable assumption for this study, as relative humidity was high (average = 77 %), and the aerosol arriving at the measurement site is often aged. The aerosol was assumed to be thermodynamically stable; i.e. the aerosol can exist as both solid and liquid, and salts are able to precipitate if the aqueous phase becomes saturated with respect to them. The ambient temperature and relative humidity data were taken from the measurements made nearby at the Sultan Ismail Petra Airport. It is likely that these measurements are representative of the Bachok research station, as further investigation of data from two other meteorological stations showed that temperature and relative humidity remain consistent along the coastline.

## 3 Results and discussion

### 3.1 Bachok demonstration campaign

The filter samples were collected at the Bachok atmospheric observation tower. The Bachok district, located in the state of Kelantan, is a rural area and the primary economic activity comes from tobacco and kenaf plantations. Other agrarian activities in the wider Kelantan region include the production of rice and rubber as well as additional economic activities such as livestock rearing and fishing. Figure 2 shows the 7-day backward air mass trajectories arriving at the measurement site during the demonstration campaign, with each trajectory coloured by the mean altitude (m). For comparison with pollutant trends later in this study, the trajectories have been separated into two plots according to their mean height. As expected during the winter months, the strong anticyclone system known as the Siberian High led to the arrival of northeasterly onshore winds along the east coast of Peninsular Malaysia. Some of the air masses experienced a

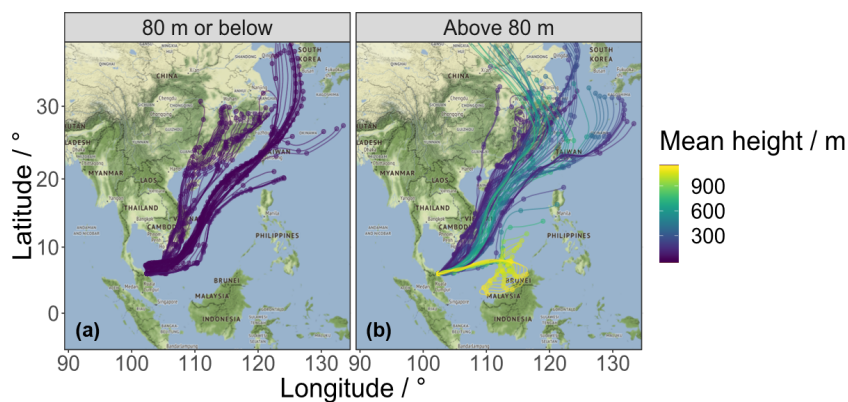


**Figure 2.** The 7-day HYSPLIT backward air mass trajectories centred on the Bachok Marine Research Station between 18 January and 7 February 2014. Each trajectory is coloured by the mean altitude (m). Trajectories with a mean height of 80 m or below are shown in panel (a) and trajectories with a mean height greater than 80 m are shown in panel (b).

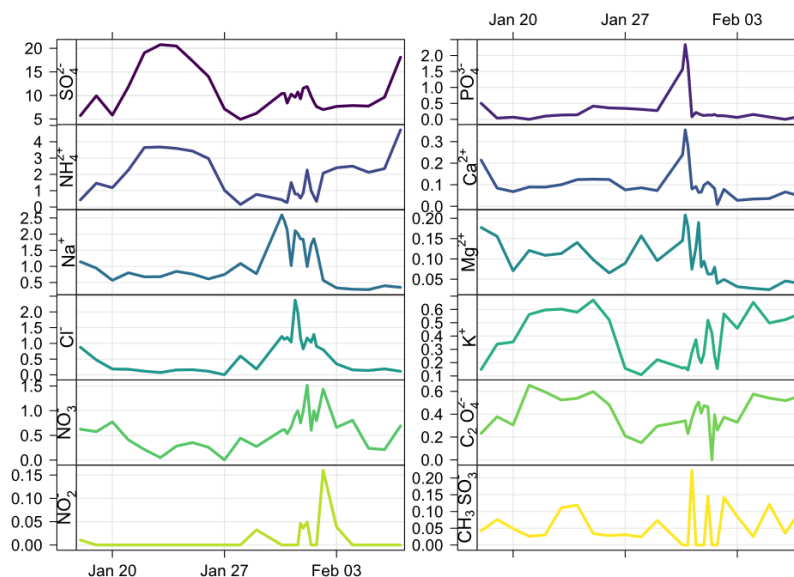


**Figure 3.** Time series of water-soluble ions ( $\mu\text{g m}^{-3}$ ) measured during the Bachok demonstration campaign (18 January to 7 February 2014).

significant continental influence from highly industrialised countries such as China, Japan, North and South Korea, and the island of Taiwan, whilst other air masses had a stronger marine influence from both the East China Sea and the South China Sea.

Although there was no reliable meteorological data recorded at the measurement site during the demonstration campaign, data from a nearby meteorological station were available. The station is located approximately 23 km away at the Sultan Ismail Petra Airport in Kota Bharu, as shown in Fig. S1 (Supplement). Whilst the meteorological data from the Airport will not be exactly representative of the measurement site, the patterns in wind direction are consistent with observations made by the field scientists during the campaign. In addition, during a study of the influence of northeast monsoon cold surges on air quality in Southeast

Asia, Ashfold et al. (2017) used meteorological data from three locations that they believed to lie in the path of cold surges during the northeast monsoon, offering the best possibility of observing a cold-surge influence on air pollution. These sites were in Kota Bharu (lat 6.141, long. 102.247), Kuala Terengganu (lat 5.308, long. 103.118) and Kemaman (lat 4.271, long. 103.428); this provides further confirmation that data from the Sultan Ismail Petra Airport site are suitable for evaluating broad-scale transport at the Bachok measurement site. Figure S2 in the Supplement shows average hourly wind speed and wind direction conditions across the entire duration of the measurement campaign (18 January to 6 February 2014). On most days, gentle southwesterlies from the land (Peninsular Malaysia) were observed in the early hours of the morning to around 11:00 LT (Malaysia time). At this stage, a dramatic shift in wind direction occurred,

**Table 1.** Mean and maximum ion concentrations measured throughout the measurement period. The average percent mass contribution of each ion to the total measured ions is included as well as the percent of samples in which each target ion is found (%Qt).

Ion	Mean (ion) $\mu\text{g m}^{-3}$	Maximum (ion) $\mu\text{g m}^{-3}$	Mean percent mass of total measured ion content	%Qt <sup>a</sup>	%RSD <sup>b</sup> <sub>total</sub>
SO <sub>4</sub> <sup>2-</sup>	10.7	20.8	65.6	100	11.2
NH <sub>4</sub> <sup>+</sup>	1.69	4.73	10.4	100	6.38
Na <sup>+</sup>	1.13	2.60	6.95	100	6.88
Cl <sup>-</sup>	0.67	2.38	4.14	100	8.49
NO <sub>3</sub> <sup>-</sup>	0.61	1.52	3.76	100	22.6
C <sub>2</sub> O <sub>4</sub> <sup>2-</sup>	0.42	0.65	2.57	97	13.9
PO <sub>4</sub> <sup>3-</sup>	0.36	2.34	2.22	93	15.4
K <sup>+</sup>	0.38	0.67	0.67	100	6.35
Ca <sup>2+</sup>	0.10	0.35	0.64	100	9.26
Mg <sup>2+</sup>	0.10	0.21	0.61	100	6.72
CH <sub>3</sub> SO <sub>3</sub> <sup>-</sup>	0.08	0.22	0.47	67	10.6
NO <sub>2</sub> <sup>-</sup>	0.05	0.16	0.33	23	14.3
Total	16.2	27.0	–	–	–

<sup>a</sup> Percentage of samples in which the target ion was above the LOQ. <sup>b</sup> Total error associated with each ion.

and until around 19:00 LT a strong onshore breeze from the northeast (South China Sea) was observed. From 20:00 LT to the early hours of each morning, a calmer sea breeze predominantly from the east was seen. Hourly VOC measurements were conducted at the measurement site, and the development of a sea breeze at approximately 11:00 LT dramatically influenced the diurnal profiles of the measured species (Fig. S3, Supplement). In the morning, when the air being sampled was coming over the land, high levels of NO, NO<sub>2</sub> and anthropogenic VOCs such as toluene and C<sub>10</sub> aliphatics were observed; the main source of these species was local burning of waste (Dunmore et al., 2016). When the sea breeze developed, the concentration of these species dropped significantly.

### 3.2 Composition of water-soluble ions in atmospheric aerosol

#### 3.2.1 Aerosol composition and determination of non-sea-salt and sea salt components

The total concentration of measured water-soluble ions in the PM<sub>2.5</sub> during the campaign ranged from 8.06 to 27.0  $\mu\text{g m}^{-3}$ , with an average concentration of 16.2  $\mu\text{g m}^{-3}$ . Table 1 shows the mean and maximum water-soluble ion concentrations measured throughout the campaign, and Fig. 3 shows time series for all the ions measured in the aerosol.

As the composition of the water-soluble ions present in aerosol collected at the Bachok site was influenced by both marine and continental sources, it is useful to make an estimation of non-sea-salt (nss) and sea salt (ss) components, using Eqs. (1)–(4). Total Na<sup>+</sup> and Ca<sup>2+</sup> concentrations have been measured in this study, and the mean Ca<sup>2+</sup>/Na<sup>+</sup> ratio

in the crust and mean Ca<sup>2+</sup>/Na<sup>+</sup> ratio in seawater have been estimated as 1.78 *w/w* and 0.038 *w/w* respectively (Bowen, 1979). Therefore it is possible to solve Eqs. (1)–(4) simultaneously for ssNa<sup>+</sup>, nssNa<sup>+</sup>, ssCa<sup>2+</sup> and nssCa<sup>2+</sup> (Boreddy and Kawamura, 2015). Furthermore, the resulting estimate of ssNa<sup>+</sup>, which can be used as a sea spray marker, can also be used to predict the contribution of nssSO<sub>4</sub><sup>2-</sup> and nssK<sup>+</sup> in the aerosol, as shown in Eqs. (5) and (6) respectively. Whilst there may be some uncertainty in the mean Ca<sup>2+</sup>/Na<sup>+</sup> crustal ratio, due to challenges associated with predicting the composition of the crust (Bowen, 1979), this approach provides more accuracy than simply using total Na<sup>+</sup> as a sea spray marker.

$$\text{ssNa}^+ = \text{Na}^+ - \text{nssNa}^+ \quad (1)$$

$$\text{nssNa}^+ = \text{nssCa}^{2+} \cdot \left( \frac{\text{Ca}^{2+}}{\text{Na}^+} \right)_{\text{crust}} \quad (2)$$

$$\text{nssCa}^{2+} = \text{Ca}^{2+} - \text{ssCa}^{2+} \quad (3)$$

$$\text{ssCa}^{2+} = \text{ssNa}^+ \cdot \left( \frac{\text{Ca}^{2+}}{\text{Na}^+} \right)_{\text{sea water}} \quad (4)$$

$$\text{nssSO}_4^{2-} = \text{SO}_4^{2-} - 0.253 \cdot \text{ssNa}^+ \quad (5)$$

$$\text{nssK}^+ = \text{K}^+ - 0.037 \cdot \text{ssNa}^+ \quad (6)$$

Figure 4 shows a series of stacked bar charts to summarise the average mass composition of water-soluble ions in atmospheric aerosol and the distribution of non-sea-salt and sea salt components. The results show that the water-soluble ion fraction of the aerosol is dominated by SO<sub>4</sub><sup>2-</sup>, which on average made up 65.6% of the total ion content by mass. NH<sub>4</sub><sup>+</sup> and NO<sub>3</sub><sup>-</sup> concentrations were significantly lower, with mean concentrations of 1.69 and 0.61  $\mu\text{g m}^{-3}$  respectively.

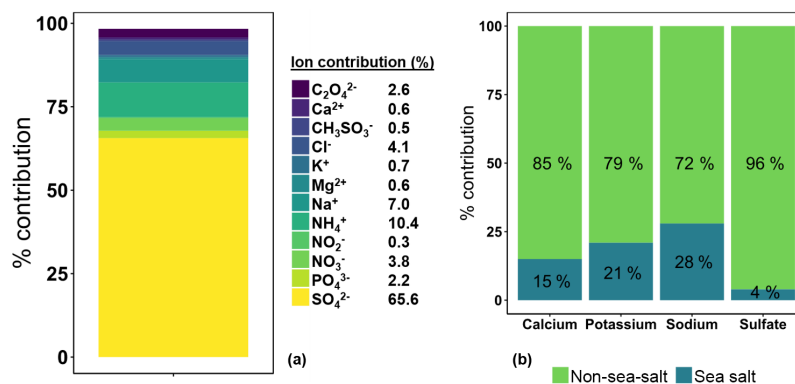


**Figure 4.** Stacked bar chart to show the average mass composition of water-soluble ions in aerosol collected at the Bachok research station (a) and stacked bar charts to show the percentage of non-sea-salt and sea salt fractions of  $\text{Ca}^{2+}$ ,  $\text{K}^+$ ,  $\text{Na}^+$  and  $\text{SO}_4^{2-}$  (b, left to right).

$\text{Na}^+$  and  $\text{Cl}^-$  made up 11.1 % of the total ion content, and 72 % of the measured  $\text{Na}^+$  was attributed to  $\text{ssNa}^+$ . The average concentrations of  $\text{nssK}^+$  and  $\text{nssCa}^{2+}$  were  $0.30$  and  $0.09 \mu\text{g m}^{-3}$  respectively; these ions can be used as tracers for biomass burning ( $\text{nssK}^+$ ) and atmospheric dust ( $\text{nssCa}^{2+}$ ).  $\text{NO}_2^-$  and  $\text{CH}_3\text{SO}_3^-$  were the least abundant ions, with average concentrations of  $0.05$  and  $0.08 \mu\text{g m}^{-3}$ . The two ions were only observed in a subset of samples;  $\text{CH}_3\text{SO}_3^-$  was quantified in 67 % of samples and quantification of  $\text{NO}_2^-$  was only achieved in 23 % of samples.

### 3.2.2 Sources and formation of sulfate ( $\text{SO}_4^{2-}$ )

The average  $\text{SO}_4^{2-}$  concentration during the measurement campaign was  $10.7 \mu\text{g m}^{-3}$ , with a maximum concentration of  $20.8 \mu\text{g m}^{-3}$  recorded. The formation of  $\text{SO}_4^{2-}$  in the particle phase occurs when emitted  $\text{SO}_2$  is oxidised by  $\text{OH}$  in the gas phase, or by  $\text{O}_3$  or  $\text{H}_2\text{O}_2$  in the aqueous phase (Fisher et al., 2011). The most dominant anthropogenic sources of  $\text{SO}_2$  include fuel and industrial emissions, as well as open biomass burning.

By using  $\text{ssNa}^+$  as a sea spray marker to determine non-sea-salt and sea salt components of the aerosol, it was found that on average 96 % of the measured  $\text{SO}_4^{2-}$  was  $\text{nssSO}_4^{2-}$ , and only 4 % of the  $\text{SO}_4^{2-}$  was from sea salt. As a potential biogenic source of  $\text{nssSO}_4^{2-}$  is DMS emissions from marine biota, and the main atmospheric source of MSA is the oxidation of DMS, it is possible to use the  $\text{MSA}^-/\text{nssSO}_4^{2-}$  ratio as a tracer to assess the contribution of biogenic sources to  $\text{nssSO}_4^{2-}$  in the atmosphere (Legrand and Pasteur, 1998). In this study,  $\text{MSA}^-$  concentrations ranged from  $0.02$  to  $0.22 \mu\text{g m}^{-3}$ , with an average concentration of  $0.08 \mu\text{g m}^{-3}$ . As a result, the  $\text{MSA}^-/\text{nssSO}_4^{2-}$  ratio ranged from  $1.6 \times 10^{-3}$  to  $2.2 \times 10^{-2}$ , with an average value of  $8.0 \times 10^{-3}$ . These values are low compared to  $\text{MSA}^-/\text{nssSO}_4^{2-}$  ratios recorded at remote sites; for example, a  $\text{MSA}^-/\text{nssSO}_4^{2-}$  mean mass ratio of  $7 \times 10^{-2}$  has been measured on Fanning Island and American Samoa (Savoie and Prospero, 1989).

The lower ratios recorded in Bachok suggest the majority of  $\text{nssSO}_4^{2-}$  at the site originates from anthropogenic sources.

As previously discussed, a study by Dunmore et al. (2016) revealed that levels of  $\text{NO}_x$  and anthropogenic VOCs at the Bachok measurement site were significantly higher when the air being sampled had passed over nearby land and dropped significantly at around 11:00 LT when a sea breeze developed. This indicated that air quality in Bachok is influenced by local sources of pollution, such as vehicle emissions and burning domestic waste. Pollution rose plots (Fig. 5) show the relationship between wind direction and speed and  $\text{SO}_2$  concentration at the Bachok measurement site. The left panel shows recorded  $\text{SO}_2$  concentrations  $\geq 5$  ppb and for comparison, the right panel shows all  $\text{SO}_2$  data recorded during the measurement period.  $\text{SO}_2$  concentrations  $< 5$  ppb have been excluded from the left panel plot to further investigate the meteorological conditions when the spikes in  $\text{SO}_2$  concentration occur. In the lower right corner of each pollution rose, “mean” represents the mean  $\text{SO}_2$  concentration and “calm” represents the fraction of data that cannot be attributed to a specific wind direction. During the elevated  $\text{SO}_2$  periods ( $\geq 5$  ppb), weak southwesterlies dominated and the average wind speed was  $1.1 \text{ m s}^{-1}$ . The mean  $\text{SO}_2$  concentration was 24.7 ppb during these events. Over the entire measurement campaign, however, average wind speed was considerably higher,  $2.8 \text{ m s}^{-1}$ , and the air arrived predominantly from the east. In summary, the majority of higher  $\text{SO}_2$  events were observed in calmer conditions when the air arriving at the site had passed over nearby land; these observations provide further evidence for the influence of local sources of pollution.

At the Bachok measurement site, no obvious relationship was observed between  $\text{SO}_2$  and particulate  $\text{SO}_4^{2-}$  concentration or between  $\text{SO}_4^{2-}$  concentration and wind direction. This is likely to be because it takes time for  $\text{SO}_2$  to oxidise to  $\text{SO}_4^{2-}$  and that the  $\text{SO}_4^{2-}$  fraction of the aerosol is more heavily influenced by long-range transport of aged emissions from East Asia. To investigate this further, the backward air mass trajectories were coloured by the concentration of

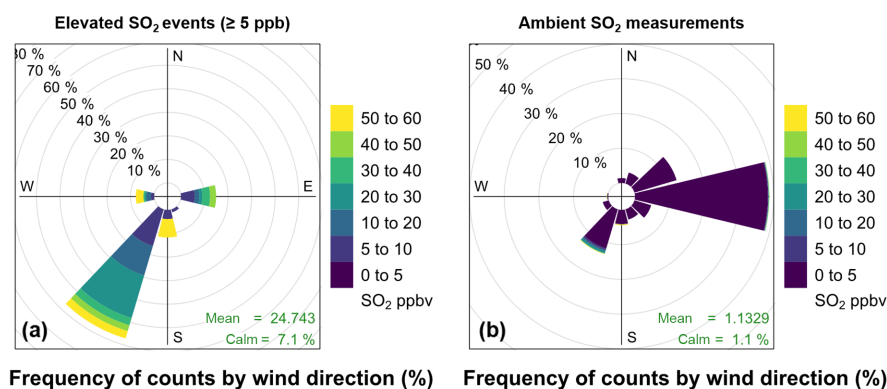


**Figure 5.** Pollution rose plots to show the relationship between wind direction and SO<sub>2</sub> concentration at the Bachok measurement site. Panel (a) represents recorded SO<sub>2</sub> concentrations  $\geq 5$  ppb and panel (b) represents all SO<sub>2</sub> data recorded during the measurement period. Plot constructed using the openair package in RStudio (Carslaw and Ropkins, 2012; Carslaw, 2015).

SO<sub>4</sub><sup>2-</sup>, as shown in Fig. 6. To allow for comparison with Fig. 1, trajectories with a mean height of 80 m or below are shown on the left panel and trajectories with a mean height greater than 80 m are shown on the right panel. At the lower altitudes ( $\leq 80$  m), it is clear that the SO<sub>4</sub><sup>2-</sup> content of the aerosol is highest (ca.  $15\text{--}20\ \mu\text{g m}^{-3}$ ) when the site is influenced by continental air masses from industrialised regions of East Asia and lower when the air masses have a more significant marine influence. This trend is less clear at higher altitudes (right panel, mean height  $> 80$  m), but nevertheless some of the lowest SO<sub>4</sub><sup>2-</sup> levels are observed ( $\sim 5\ \mu\text{g m}^{-3}$ ) when marine air that has passed over the East and South China seas arrives at the site. With this information available, it is useful to perform cluster analysis on the back trajectories; this type of analysis groups air masses of similar geographic origin together, which provides more information on pollutant species with similar chemical histories. A distance matrix is used to create a specified number of clusters with the most different air mass pathways. Figure 7 shows the five-cluster solution to back trajectories calculated for the Bachok site during the measurement campaign.

Clusters 1 and 3 were associated with mean SO<sub>4</sub><sup>2-</sup> concentrations of  $14.4$  and  $13.8\ \mu\text{g m}^{-3}$  respectively. The mean altitude of cluster 1 was 72 m and the mean altitude of cluster 3 was 501 m. Full details of the air mass trajectories within each cluster are detailed in the Supplement (Table S3). These clusters contained air masses that had passed over several highly industrialised regions en route to Bachok, including cities such as Guangzhou (China) and Ho Chi Minh City (Vietnam). Average SO<sub>4</sub><sup>2-</sup> concentrations for clusters 2 and 4 were  $8.4$  and  $8.3\ \mu\text{g m}^{-3}$ , with mean altitudes of 169 and 37 m respectively. These air masses are likely to have experienced some continental influence from the east coast of China and the island of Taiwan but have a much more significant marine influence from passing over the South China Sea before arriving at Bachok. For air masses within clusters 1–4, the concentration of SO<sub>4</sub><sup>2-</sup> increases with decreasing

altitude and increasing influence from industrialised regions. The mean altitude of air masses within cluster 5 was 1027 m, i.e. significantly higher than air masses in clusters 1–4. Furthermore, the air masses in cluster 5 arriving at the site were not a result of northeasterly monsoon winds from East Asian countries travelling across the South China Sea. Instead, there is evidence of a cyclonic weather system off the coast of the island of Borneo over the South China Sea. The air masses in cluster 5 arrived during the final 24 h period of the measurement campaign, and only one SO<sub>4</sub><sup>2-</sup> measurement is available ( $18.1\ \mu\text{g m}^{-3}$ ). It is not possible to fully understand the nature of air masses from this different region without further measurements.

Despite potential differences in atmospheric lifetimes and behaviour, other pollutants aside from SO<sub>4</sub><sup>2-</sup> can provide further evidence that substantial amounts of industrial pollution from East Asia are undergoing atmospheric transport to tropical regions of the Western Pacific. For example, Oram et al. (2017) measured chlorine-containing, very short-lived substances (Cl-VSLs) at the Bachok research station during the winter monsoon season in late January–early February 2014. Cl-VSLs are ozone-depleting species with short atmospheric lifetimes, typically less than 6 months. Species include dichloromethane (CH<sub>2</sub>Cl<sub>2</sub>) and 1,2-dichloroethane (CH<sub>2</sub>ClCH<sub>2</sub>Cl). A 7-day pollution or cold-surge event was reported between 19 and 26 January 2014, when significantly enhanced concentrations of Cl-VSLs were observed. During this pollution episode, the measured samples were heavily impacted by emissions from the East Asian mainland, whilst this influence was less significant during the cleaner, non-polluted periods. In fact, the total median concentration of the four measured Cl-VSLs was 546 ppt between 20 and 26 January and 243 ppt during the less polluted period (27 January to 5 February 2014). Oram et al. (2017) noted that even after the cold-surge event, the levels of Cl-VSLs were still significantly higher than expected, indicating that this region of the South China Sea is widely im-



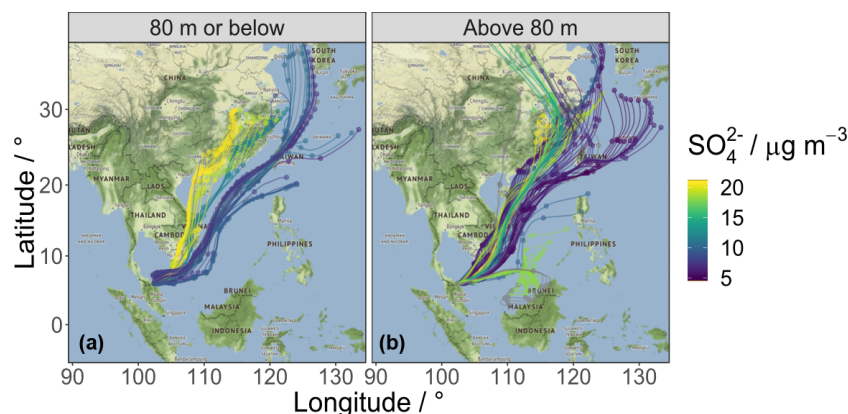


**Figure 6.** The 7-day HYSPLIT backward air mass trajectories centred on the Bachok research station between 18 January and 7 February 2014. The back trajectories are coloured by the concentration of  $\text{SO}_4^{2-}$  ( $\mu\text{g m}^{-3}$ ). Trajectories with a mean height of 80 m or below are shown in panel (a) and trajectories with a mean height greater than 80 m are shown in panel (b).

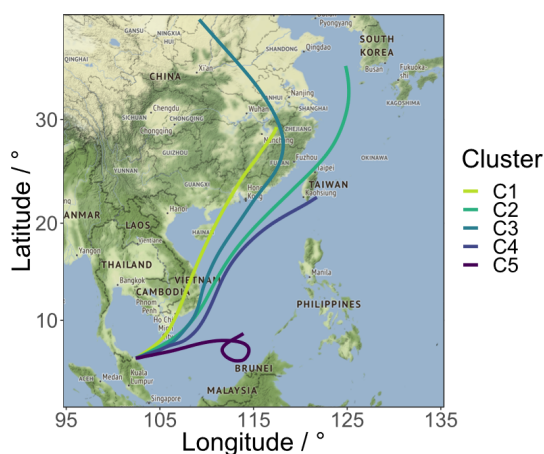


**Figure 7.** Five-cluster solution to backward air mass trajectories centred on the Bachok research station between 18 January and 7 February 2014.

ected by emissions from East Asia. Many other chemical pollutants, aside from short-lived chlorinated gases, will be present in these air masses from East Asia and will have a large impact on regional air quality. Oram et al. (2017) performed a Numerical Atmospheric dispersion Modelling Environment (NAME) trajectory analysis using carbon monoxide (CO) as a tracer of industrial emissions from regions north of  $20^\circ\text{N}$  for six winter seasons (2009–2010 to 2014–2015). A strong correlation between CO and  $\text{CH}_2\text{Cl}_2$  (a measured CI-VSLS) was observed during the pollution episode in late January 2014. Analysis of CO time series over the six winter seasons revealed that cold-surge events are likely to be repeated regularly each winter, demonstrating that pollution rapidly undergoes long-range transport across the South China Sea on a regular basis during the northeast monsoon.

### 3.2.3 Correlation of $\text{SO}_4^{2-}$ with $\text{NH}_4^+$ and implications for aerosol acidity

Ammonium ( $\text{NH}_4^+$ ) was the second most abundant ion in the aerosol; on average it made up 10.4 % of the total ion content, and the mean and maximum concentrations were 1.69 and  $4.73 \mu\text{g m}^{-3}$  respectively. The strong positive correlation between  $\text{SO}_4^{2-}$  and  $\text{NH}_4^+$  was observed ( $R = 0.77$ ,  $p < 0.001$ ). A similar observation was reported by Keyword et al. (2003) during an investigation of the sources of particles contributing to haze in the Klang Valley, Malaysia. The strong relationship between these species is due to neutralisation of  $\text{SO}_4^{2-}$  by  $\text{NH}_4^+$ . Local sources of  $\text{NH}_3$  in the rural Bachok region are likely to come from agricultural practices such as animal husbandry, fertiliser use and agricultural waste burning. The average  $\text{NH}_4^+/\text{SO}_4^{2-}$  molar ratio was 0.81, which indicated that there was insufficient gaseous  $\text{NH}_3$  in the atmosphere to neutralise  $\text{SO}_4^{2-}$ . Under an ammonia-poor regime, the uptake of  $\text{SO}_4^{2-}$  is preferential to the uptake of  $\text{NO}_3^-$  because sulfuric acid has a lower vapour pressure than nitric acid (Seinfeld and Pandis, 2006). Although measurements of the total amounts of ammonia and sulfate in the gas, aqueous and solid phases would provide a better prediction of the aerosol acidity, the results presented in this study indicated that an ammonia-poor regime exists and that the aerosol is likely to be acidic. In these scenarios, the  $\text{NH}_3$  partial pressure is low, and therefore the  $\text{NH}_3\text{-HNO}_3$  partial pressure product is also low, meaning that the concentrations of ammonium nitrate are low or zero (Seinfeld and Pandis, 2006). This hypothesis can be supported by the fact that  $\text{NO}_3^-$  concentrations in this study were very low, ranging from 0.005 to  $1.52 \mu\text{g m}^{-3}$ . As a result,  $\text{NO}_3^-$  made up a significantly smaller fraction of the total ion content compared to  $\text{SO}_4^{2-}$ ; the average percentage mass composition of the total ion content was 3.8 % for  $\text{NO}_3^-$  and 65.6 % for  $\text{SO}_4^{2-}$ .

To estimate proton loading in atmospheric particles, the strong acidity approach can be used, as shown in Eq. (7). This approach assumes that any deficit in measured cation charge compared to measured anion charge can be attributed to  $H^+$ . Total anion and total cation equivalents can be estimated using Eqs. (8) and (9).

$$\text{strong acidity } (\mu\text{eq. m}^{-3}) = \sum \text{anion eqivs. } (\mu\text{eq. m}^{-3}) - \sum \text{cation eqivs. } (\mu\text{eq. m}^{-3}) \quad (7)$$

$$\sum \text{anion eqivs. } (\mu\text{eq. m}^{-3}) = \frac{\text{SO}_4^{2-}}{48} + \frac{\text{NO}_3^-}{62} + \frac{\text{Cl}^-}{35.5} + \frac{\text{PO}_4^{3-}}{31.6} + \frac{\text{C}_2\text{O}_4^{2-}}{44} + \frac{\text{NO}_2^-}{46} + \frac{\text{CH}_3\text{SO}_3^-}{95} \quad (8)$$

$$\sum \text{cation eqivs. } (\mu\text{eq. m}^{-3}) = \frac{\text{Na}^+}{23} + \frac{\text{NH}_4^+}{18} + \frac{\text{K}^+}{39} + \frac{\text{Mg}^{2+}}{12} + \frac{\text{Ca}^{2+}}{20} \quad (9)$$

As shown in Fig. 8, strong acidity values ranged from 0.03 to  $0.19 \mu\text{eq. m}^{-3}$ , with an average value of  $0.11 \mu\text{eq. m}^{-3}$ . The positive strong acidity values provide an initial indication that the aerosol is acidic and allows an estimate of the proton loading to be made (average  $H^+ = 0.11 \mu\text{g m}^{-3}$ ).

To obtain error bars for the strong acidity predictions (Fig. 8),  $H_{\text{max}}^+$  and  $H_{\text{min}}^+$  were calculated according to Eqs. (10) and (11) respectively. For  $H_{\text{max}}^+$  the anions were adjusted up to within their uncertainties (i.e.  $+\%RSD_{\text{tot}}$ ), and the cations were adjusted down to within their uncertainties (i.e.  $-\%RSD_{\text{tot}}$ ). For  $H_{\text{min}}^+$  the anions were adjusted down and the cations were adjusted up (Murphy et al., 2017). The  $\%RSD_{\text{tot}}$  value was estimated by combining the error of the recovery process for each ion ( $\%RSD_{\text{rec}}$ , Table S1) and the error of the instrument for each ion ( $\%RSD_{\text{ins}}$ , Table S2).

$$H_{\text{max}}^+ = \sum \text{max anion equivalents} - \sum \text{min cation equivalents} \quad (10)$$

$$H_{\text{min}}^+ = \sum \text{min anion equivalents} - \sum \text{max cation equivalents} \quad (11)$$

In most cases,  $H_{\text{min}}^+$  remains above zero. However, between 2 and 6 February 2014, slightly negative  $H_{\text{min}}^+$  values between  $-1 \times 10^{-3}$  and  $-2 \times 10^{-2} \mu\text{eq. m}^{-3}$  were calculated, which are physically implausible (Murphy et al., 2017). These results highlight the possible sources of error associated with the strong acidity approach for estimating aerosol acidity. For example, Hennigan et al. (2015) report that organic acids (which are mostly excluded from this study, except for MSA and oxalic acid) can have an important influence on aerosol acidity, especially at relatively low acidities where organic acids dissociate and contribute to the ion balance. Furthermore, they can form salt complexes with inorganic species e.g. ammonium oxalate. Neglecting organic acids, as well as

other atmospheric species such as  $\text{HCO}_3^-$  and basic amines, will lead to inaccuracies in the calculated  $H^+$ .

Thermodynamic equilibrium models such as ISORROPIA II can also be used to predict aerosol pH (Fountoukis and Nenes, 2007). The ambient temperature and relative humidity data recorded nearby at the Sultan Ismail Petra Airport were assumed to be representative of the Bachok research station, as further investigation of data from two other meteorological stations revealed that temperature and relative humidity remained consistent. A map to show the location of the three meteorological stations along the east coast, as well as the Bachok research station, can be found in the Supplement (Fig. S1). The two other stations are Narathiwat Airport (lat 6.520, long. 101.743) and Sultan Mahmud Airport (lat 5.383, long. 103.103). Average relative humidity between 18 January and 7 February 2014 was 77.7 % at Sultan Petra Ismail Airport, 75.4 % at Narathiwat Airport and 77.0 % at Sultan Mahmud Airport. Average temperatures recorded at the stations during this time were 24.8, 25.6 and 25.4 °C for Sultan Petra Ismail, Sultan Mahmud and Narathiwat airports respectively.

The ISORROPIA II thermodynamic model predictions of  $\text{PM}_{2.5}$  pH are shown in Fig. 9. Particle pH was estimated with ISORROPIA II run in the reverse mode without gas phase species input and ranged from  $-0.97$  to  $1.12$  during the measurement period, implying that the aerosol was highly acidic. The pH prediction for the aerosol collected between midday on 3 and 4 February 2014 was 7.06 and has been excluded from Fig. 9. The particle concentrations input on this day correspond to negative values of strong acidity, and therefore the model balances charge by assuming  $[\text{OH}^-] > [\text{H}^+]$ ; this leads to a calculated pH of greater than 7. Murphy et al. (2017) reported that pH prediction is sensitive to strong acidity in the limit of strong acidity approaching zero and that the model can be drastically improved if gas phase  $\text{NH}_3$  and  $\text{HNO}_3$  measurements are included. The gas-to-particle partitioning of these species is sensitive to pH under conditions commonly encountered in the atmosphere; therefore gaseous  $\text{NH}_3$  and  $\text{HNO}_3$  measurements provide better constraint on the thermodynamic model.

Acidic particles can have detrimental effects on human health, air quality, and the health of aquatic and terrestrial ecosystems (Hennigan et al., 2015). For example, Gwynn et al. (2000) performed a time-series analysis of acidic PM and daily mortality and morbidity in the Buffalo, New York, region; several significant pollutant–health effect associations were identified, the strongest being the correlation between atmospheric  $\text{SO}_4^{2-}$  concentration and respiratory hospital admissions. Furthermore, particle acidity can influence various atmospheric chemical processes, including  $\text{SO}_2$  oxidation, halogen chemistry, and the partitioning of ammonia, nitric acid, organic acids and isomeric epoxy diols from isoprene photooxidation (IEPOX) (Hennigan et al., 2015; Surratt et al., 2010; Lin et al., 2012). In summary, whilst some of the risks associated with aerosol acidity in Bachok origi-

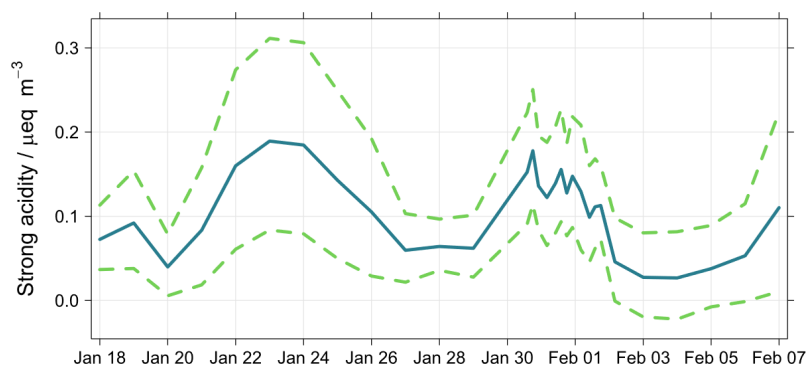


**Figure 8.** Predictions of particle strong acidity for the aerosol collected during the Bachok measurement campaign. Dashed lines represent predictions of minimum and maximum limits of strong acidity.

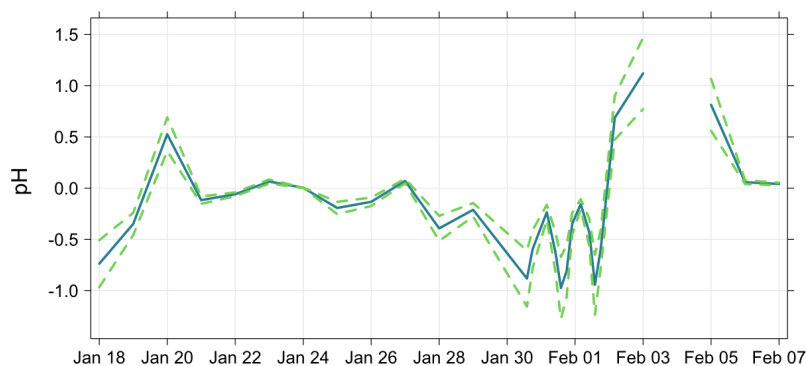


**Figure 9.** Predicted  $\text{PM}_{2.5}$  pH at the Bachok measurement site using ISORROPIA II (Fountoukis and Nenes, 2007). Dashed lines represent predictions of minimum and maximum limits of pH.

nate from local sources of pollution, it is possible that people living in these rural areas are also exposed to an additional risk, as the region appears to be sensitive to the effects of industrialisation further afield in East Asia.

### 3.2.4 Sources and formation of oxalate, $\text{C}_2\text{O}_4^{2-}$

Oxalic acid is the most abundant dicarboxylic acid in tropospheric aerosol (Sareen et al., 2016). This major water-soluble organic component can alter the hygroscopicity of aerosols and can either act as cloud condensation nuclei (CCN), or reduce the surface tension of particles to form CCN (Saxena and Hildemann, 1996; Novakov and Penner, 1993; Facchini et al., 1999; Kerminen, 2001). In this study, oxalate made up 2.6% of the total measured water-soluble ion content. The average concentration was  $0.42 \mu\text{g m}^{-3}$ , and throughout the measurement period the concentration ranged from 0.15 to  $0.65 \mu\text{g m}^{-3}$ . Interestingly, such levels of oxalate in atmospheric aerosol are typical of urban environments, despite the fact that the Bachok research station is located in a rural coastal region. For example, Freitas et al. (2012) report average oxalate concentrations in  $\text{PM}_{10}$  at an urban site and a rural site in Londrina city, Brazil, of 0.57 and  $0.03 \mu\text{g m}^{-3}$  respectively. Other reported oxalate con-

centrations in urban TSPs (total suspended particles) include measurements of  $0.10\text{--}0.48 \mu\text{g m}^{-3}$  in Shanghai (Jiang et al., 2011) and  $0.27 \mu\text{g m}^{-3}$  in Tokyo (Sempere and Kawamura, 1994).

To investigate possible oxalate sources and formation pathways, it is necessary to consider the correlation of oxalate with different atmospheric species. Jiang et al. (2011) report using  $\text{NO}_2^-$  as an indicator for vehicle emissions,  $\text{nssSO}_4^{2-}$  and  $\text{NO}_3^-$  for secondary formation through different pathways, and  $\text{K}^+$  for biomass burning. A study carried out by Huang et al. (2006) in the urban area of Shenzhen (Southern China) reported that, whilst good correlation of droplet oxalate with  $\text{K}^+$  was observed ( $R^2 = 0.75$ , average diameter:  $1.0 \mu\text{m}$ ), there was poor correlation between oxalate and  $\text{K}^+$  in the condensation mode ( $R^2 = 0.10$ , average diameter:  $0.4 \mu\text{m}$ ). This implied that whilst biomass burning was probably not an important primary source of condensation mode oxalate, it is likely that biomass burning particles act as effective CCN, promoting in-cloud sulfate and oxalate formation. In this study,  $\text{nssK}^+$  levels remained below  $0.7 \mu\text{g m}^{-3}$ ; this likely represents background biomass burning emissions over the region during the measurement period, as evidenced by fire hotspots from satellite data shown in Fig. S4 (Giglio et al., 2003). A strong correlation was ob-

served between oxalate and  $\text{nssK}^+$  ( $R = 0.78$ ,  $p < 0.001$ ), and the oxalate /  $\text{nssK}^+$  ratio ranged from 0.68 to 4.64 during the Bachok measurement campaign. These ratios are significantly higher than those found in aerosol directly emitted from vegetation fires in the Amazon Basin (Yamasoe et al., 2000), suggesting that biomass burning in the wider region influenced the secondary formation of oxalate, rather than acting as a primary source. A similar hypothesis was proposed by Huang and Yu (2007), who measured ambient  $\text{PM}_{2.5}$  in an urban environment in the Pearl River Delta region of China, and reported oxalate /  $\text{K}^+$  ratios of 0.57 and 0.33 in summer and winter respectively. It is worth noting that whilst the higher ratios reported in both studies indicate that biomass burning is not a major primary source of oxalate, measurements of oxalate and  $\text{K}^+$  in local biomass burning aerosols (rather than aerosol in the Amazon Basin) would provide a better indication of the source contribution by biomass burning.

There was no significant correlation observed between oxalate and  $\text{NO}_3^-$ , or between oxalate and  $\text{NO}_2^-$ . The lack of correlation with  $\text{NO}_3^-$  suggests that the two species do not have similar formation pathways and that vehicle emissions are not an important secondary source of oxalate. It is also unlikely that vehicle emissions contribute to the primary sources of oxalate, due to the lack of correlation between oxalate and  $\text{NO}_2^-$ . However,  $\text{NO}_2^-$  was only detected in 7 out of the 30 samples collected, so it is difficult to ascertain whether there is a relationship between these two species or not. A strong correlation between oxalate and  $\text{nssSO}_4^{2-}$  ( $R = 0.69$ ,  $p < 0.001$ ) was observed, suggesting a common formation pathway of the two species. It is well known that  $\text{SO}_4^{2-}$  forms via aqueous oxidation (Seinfeld and Pandis, 2006), and modelling studies also suggest that aqueous chemistry is a large contributor of oxalate formation globally (Myriokefalitakis et al., 2011). Furthermore, Carlton et al. (2006) report that whilst there are likely to be many sources of oxalate, oxidation of pyruvate in the aqueous phase is known to form oxalate at dilute (cloud-relevant) concentrations. Tan et al. (2012) also state that aqueous acetate oxidation is a key source of oxalate. A positive correlation between oxalate and  $\text{NH}_4^+$  was also observed ( $R = 0.73$ ,  $p < 0.001$ ). A similar observation was reported by Jiang et al. (2011) in a study of aerosol oxalate in Shanghai. Using size distribution data, they were able to propose that the correlation was due to the presence of ammonium oxalate in the aerosol. In this study there are no size distribution data available, and so it is important to consider the fact that the correlation may be linked to the influence of sulfate on both  $\text{NH}_4^+$  and oxalate in aerosol;  $\text{NH}_4^+$  partitions to the aerosol from gaseous  $\text{NH}_3$  in an attempt to neutralise acidic sulfate particles, whilst oxalate exhibits similar formation pathways to  $\text{SO}_4^{2-}$ .

### 3.2.5 Sea salt aerosol and factors affecting chloride depletion

On average,  $\text{Na}^+$  and  $\text{Cl}^-$  contributed 7.0 % and 4.1 % to the total measured water-soluble ion content respectively, and 72 % of the measured  $\text{Na}^+$  was attributed to  $\text{ssNa}^+$ . The concentration of  $\text{ssNa}^+$  ranged from 0.24 to 2.35  $\mu\text{g m}^{-3}$ , whilst the concentration of  $\text{Cl}^-$  ranged from 0.003 to 2.38  $\mu\text{g m}^{-3}$ . There was no correlation between  $\text{nssNa}^+$  and  $\text{Cl}^-$  ( $R = -0.01$ ), but a strong positive correlation between  $\text{ssNa}^+$  and  $\text{Cl}^-$  was observed ( $R = 0.84$ ,  $p < 0.001$ ). During the measurement period, the  $\text{Cl}^-/\text{ssNa}^+$  molar ratio ranged from 0.003 to 1.10 with an average value of 0.40. A time series of  $\text{Cl}^-/\text{ssNa}^+$  molar ratio can be found in the Supplement (Fig. S5). Significant  $\text{Cl}^-$  depletion was observed, as all of the ratios recorded were lower than that of bulk seawater, 1.18 (Boreddy and Kawamura, 2015). Figure 10 shows backward air mass trajectories arriving at the Bachok research station, coloured by the  $\text{Cl}^-/\text{ssNa}^+$  molar ratio.

A study of marine aerosol at the remote Chichi-jima island in the western North Pacific during 2001 and 2002 reported that mean  $\text{Cl}^-/\text{Na}^+$  molar ratios were highest (1.34) in September 2001 and lowest (0.30) in May 2002, and the mean ratio across the 2-year period was 1.10 (Boreddy et al., 2014). Boreddy et al. (2014) reported that the observed chloride depletion was likely due to acid displacement occurring as a result of atmospheric mixing of anthropogenic pollutants such as  $\text{SO}_x$  and  $\text{NO}_x$ . Acid displacement can occur when sea salt particles react with acids such as  $\text{H}_2\text{SO}_4$ ,  $\text{HNO}_3$ , oxalic acid ( $\text{C}_2\text{H}_2\text{O}_4$ ) and methanesulfonic acid ( $\text{CH}_3\text{SO}_3\text{H}$ ) in the atmosphere. Such processes are of atmospheric importance as they lead to the formation of gaseous HCl and potentially affect acid deposition conditions in the region. It is widely accepted that  $\text{Cl}^-$  depletion through the volatilisation of HCl via acid displacement occurs particularly in polluted marine air masses (Newberg et al., 2005; Sturges and Shaw, 1993). In this study, the lowest  $\text{Cl}^-/\text{ssNa}^+$  ratios were observed when air masses arriving at the site had previously passed over highly industrialised countries such as China and Vietnam (Fig. 10). Higher  $\text{Cl}^-/\text{ssNa}^+$  ratios are found in marine air masses from less polluted regions. It is possible that aerosol, particularly in northern China, may be rich in chloride in the winter due to coal burning. However, this study suggests that the influence of other anthropogenic pollutants, such as  $\text{HNO}_3$  and  $\text{H}_2\text{SO}_4$ , means that as the air is transported over the South China Sea to the Bachok region, significant  $\text{Cl}^-$  depletion can occur prior to arrival at the measurement site. In a more recent study, Boreddy and Kawamura performed regression analysis between the  $\text{Cl}^-/\text{Na}^+$  mass ratio and various acidic species, including  $\text{nssSO}_4^{2-}$ ,  $\text{NO}_3^-$ ,  $\text{MSA}^-$  and oxalic acid. They found a moderate negative correlation between  $\text{Cl}^-/\text{Na}^+$  mass ratio and  $\text{nssSO}_4^{2-}$ , and a moderate to weak negative correlation with  $\text{NO}_3^-$ ; this suggested that sulfate had a higher influence on chloride depletion than nitrate. Furthermore, whilst  $\text{MSA}^-$  moderately

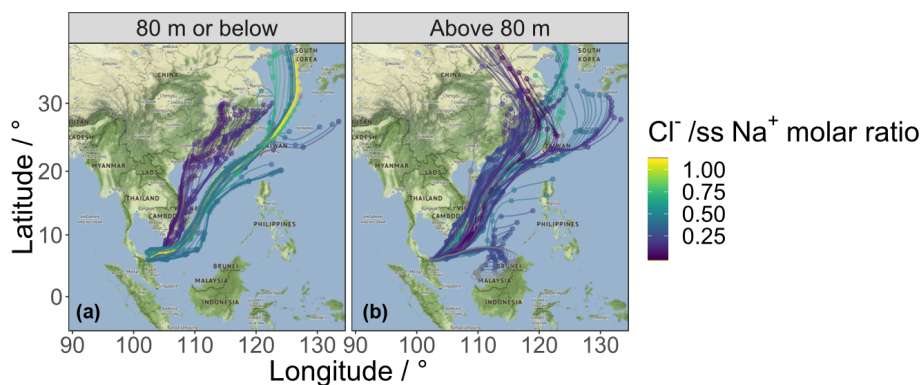


**Figure 10.** The 7-day HYSPLIT back trajectories centred on the Bachok research station, between 18 January and 7 February 2014. The back trajectories are coloured by the  $\text{Cl}^-/\text{ssNa}^+$  molar ratio. Trajectories with a mean height of 80 m or below are shown in panel (a) and trajectories with a mean height greater than 80 m are shown in panel (b).

correlated with the  $\text{Cl}^-/\text{Na}^+$  mass ratio in the summer, there was a significant negative correlation between oxalic acid and the mass ratio in the other three seasons, providing confirmation that oxalic acid plays an important role in chloride loss at Chichi-jima island. A similar regression analysis was carried out on the measurements obtained during the Bachok measurement campaign, and whilst a weak negative correlation was found between  $\text{SO}_4^{2-}$  and the  $\text{Cl}^-/\text{ssNa}^+$  mass ratio ( $R = -0.41$ ,  $p < 0.001$ ), there was no correlation of the  $\text{Cl}^-/\text{ssNa}^+$  mass ratio with oxalate or  $\text{MSA}^-$ . These results imply that whilst  $\text{H}_2\text{SO}_4$  played an important role in chloride depletion, methanesulfonic acid and oxalic acid may not have. Interestingly, a strong positive correlation was observed between  $\text{NO}_3^-$  and  $\text{Cl}^-/\text{ssNa}^+$  mass ratio ( $R = 0.82$ ,  $p < 0.001$ ). These measurements may be linked to each other through the important role of  $\text{H}_2\text{SO}_4$  in the atmosphere. Acid displacement, when sea salt reacts with  $\text{H}_2\text{SO}_4$ , leads to the removal of  $\text{Cl}^-$  from the aerosol as gaseous  $\text{HCl}$ , and a partitioning of  $\text{SO}_4^{2-}$  to the aerosol as  $\text{Na}_2\text{SO}_4$ . Furthermore, under an ammonia-poor regime (as observed in this study),  $\text{H}_2\text{SO}_4$  has a lower vapour pressure than  $\text{HNO}_3$ , leading to the preferential formation of ammonium sulfate over ammonium nitrate when there is insufficient  $\text{NH}_3$  available to fully neutralise sulfate and nitrate (Seinfeld and Pandis, 2006).

### 3.2.6 Using $\text{nssCa}^{2+}$ as a potential tracer for dust episodes

$\text{nssCa}^{2+}$  can be used as a tracer for atmospheric dust (Boreddy and Kawamura, 2015). The average concentration of  $\text{nssCa}^{2+}$  during the measurement campaign was  $0.07 \mu\text{g m}^{-3}$ , and the maximum concentration recorded was  $0.28 \mu\text{g m}^{-3}$ . On most days, the  $\text{nssCa}^{2+}$  concentration was below  $0.10 \mu\text{g m}^{-3}$ , but between midday on 30 January 2014 and midnight on 31 January 2014 (local time), elevated  $\text{nssCa}^{2+}$  levels were observed, and the average concentration during this period was  $0.22 \mu\text{g m}^{-3}$ . The same trend was observed for  $\text{PO}_4^{3-}$ ; the average concentration across the entire

measurement period was  $0.34 \mu\text{g m}^{-3}$ , but during this 12 h episode the  $\text{PO}_4^{3-}$  concentration increased to  $1.88 \mu\text{g m}^{-3}$ . The increase in ion concentration was less pronounced for  $\text{nssNa}^+$  and  $\text{Mg}^{2+}$ , but the concentrations were still  $0.26$  and  $0.88 \mu\text{g m}^{-3}$  above the average for the whole measurement period respectively. Time-series plots for  $\text{nssCa}^{2+}$ ,  $\text{PO}_4^{3-}$ ,  $\text{Mg}^{2+}$  and  $\text{nssNa}^+$  can be found in the Supplement (Fig. S6).

Between midday on 30 January 2014 and midnight on 31 January 2014, the contribution of  $\text{nssCa}^{2+}$  to the total measured water-soluble ion content was more significant (1.26 %) than the average contribution during the remainder of the measurement period (0.35 %). The Bachok research station is located in the outflow region of Asian dusts, and these measurements suggest that long-range transport of Asian dusts over the measurement site has occurred during this time. In fact, during this episode, the back trajectories arriving at the site can be traced back to the North China Plains and the Horqin Desert in eastern China; source attribution studies by Ginoux et al. (2012) have revealed that large anthropogenic dust sources are found in these regions. In the future, it is important that longer term measurements are carried out at the Bachok research station to provide confirmation that dust episodes in these regions of Asia are responsible for the elevated levels of  $\text{nssCa}^{2+}$  and other associated ions. Dust is one of the most abundant types of aerosol in the atmosphere and can have important impacts on both air quality and climate; therefore it is important that seasonal and annual trends in water-soluble ions are studied in more detail at the Bachok research station.

## 4 Conclusions

An accurate and reliable technique relying on ion chromatography has been used to make time-resolved measurements of water-soluble ions in atmospheric aerosol at the Bachok Marine Research Station. Using meteorological data from the nearby airport and HYSPLIT backward air mass trajectories

centred on the Bachok research station, it was possible to observe the diurnal wind pattern behaviour and assess where the air masses arriving at the site originated from. Air quality at this remote location is influenced by local anthropogenic and biogenic emissions, as well as marine air masses from the South China Sea and aged emissions transported from highly polluted East Asian regions during the winter monsoon season. In general, the site was influenced by south-westerlies coming from the land from the early hours of the morning until approximately 11:00 LT, and then a dramatic shift in wind direction occurred and a sea breeze was present for the remainder of the day. This shift was accompanied by a drop in the concentrations of  $\text{NO}_x$  and anthropogenic VOCs (Dunmore et al., 2016).

Twelve atmospheric water-soluble ions were measured in this study, and  $\text{SO}_4^{2-}$  was found to be the most dominant ion present, making up 66 % of the total measured ion content on average. The non-sea-salt and sea salt components of  $\text{SO}_4^{2-}$ ,  $\text{Na}^+$ ,  $\text{K}^+$  and  $\text{Ca}^{2+}$  were determined, and it was found that 96 % of the measured  $\text{SO}_4^{2-}$  was non-sea-salt  $\text{SO}_4^{2-}$ . Predictions of aerosol pH were made using the ISORROPIA II thermodynamic model and it was estimated that the aerosol was highly acidic, with pH values ranging from  $-0.97$  to  $1.12$ ; such levels of acidity are likely to have a detrimental impact on human health and the health of ecosystems at this remote coastal location. A clear difference in aerosol composition was found between continental air masses originating from industrialised regions of East Asia and marine air masses predominantly influenced by the South China Sea. For example, elevated  $\text{SO}_4^{2-}$  concentrations were observed when continental air masses that had passed over highly industrialised regions of East Asia arrived at the measurement site.

Correlation analyses amongst ionic species and assessment of ratios between different ions provided an insight into common sources and formation pathways of key atmospheric ions. Oxalate concentrations were recorded and found to be more comparable to measurements made at urban locations rather than rural ones. A strong correlation of  $\text{C}_2\text{O}_4^{2-}$  with  $\text{SO}_4^{2-}$  suggested a common aqueous oxidation formation pathway. A strong correlation between  $\text{C}_2\text{O}_4^{2-}$  and  $\text{K}^+$  coupled with high  $\text{C}_2\text{O}_4^{2-}/\text{nssK}^+$  ratios indicated that biomass burning was an important secondary source of oxalate in the Bachok region, whereas a lack of correlation with  $\text{NO}_2^-$  and  $\text{NO}_3^-$  suggested that vehicular emissions were not an important source. The average  $\text{Cl}^-/\text{nssNa}^+$  molar ratio during the measurement campaign was  $0.40$ , significantly lower than that of bulk seawater ( $1.18$ ). Analysis of back trajectories revealed that chloride depletion was greater when the aerosol was more influenced by anthropogenic sources of pollution. Elevated levels of  $\text{nssCa}^{2+}$  and other ions such as  $\text{PO}_4^{3-}$ ,  $\text{Mg}^{2+}$  and  $\text{nssNa}^+$  were observed between midday on 30 January 2014 and midnight on 31 January 2014. Assuming that  $\text{nssCa}^{2+}$  can be used as a tracer for atmospheric dust, it was proposed that the increased concentrations were

a result of air masses arriving at the site from the North China Plains and Horqin Desert. Longer term measurements are required to fully investigate the influence of Asian dusts at this remote coastal location.

To our knowledge, time-resolved measurements of water-soluble ions in  $\text{PM}_{2.5}$  are virtually non-existent in rural locations on the east coast of Peninsular Malaysia. The data presented in this study have demonstrated the capabilities of the new atmospheric tower at the Bachok research station and has provided an initial insight into factors affecting aerosol composition on this coastline. In the future, it is important that longer term measurements are carried out, with increased time-resolved sampling and particle size fractionation, to provide a better understanding of the factors affecting aerosol composition at this measurement site. This remote location is susceptible to the effects of local, regional and international air pollution, and rapid industrialisation in East Asia is influencing air quality along the east coast of Peninsular Malaysia.

*Data availability.* Raw data are available on PURE (<https://doi.org/10.15124/bd4a9045-832b-4ff8-aecc-ef1653603f1d>; Farren et al., 2018).

*Supplement.* The supplement related to this article is available online at: <https://doi.org/10.5194/acp-19-1537-2019-supplement>.

*Author contributions.* All authors contributed to the final version of this article. NJF analysed the aerosol samples and wrote the paper under the supervision of JFH. RED collected the aerosol samples, and BJB made the  $\text{SO}_2$  measurements. MIM, MSMN, AAS and SMP coordinate and manage the University of Malaya BMRS. WTS coordinated the Bachok demonstration “International Opportunities Fund” campaign.

*Competing interests.* The authors declare that they have no conflict of interest.

*Acknowledgements.* The financial support of the Natural Environment Research Council (Naomi J. Farren, PhD studentship NE/L501751/1) is gratefully acknowledged. Naomi J. Farren would like to thank David Carslaw and Will Drysdale for their assistance using R. All authors would like to acknowledge NERC (NE/J016012/1 and NE/J016047/1) for funding the Bachok demonstration “International Opportunities Fund” campaign and HICoE-MoHE IOES-2014 (Air-Ocean-Land Interactions) for supporting the Bachok Marine Research Station facilities.

Edited by: Hang Su

Reviewed by: two anonymous referees

## References

- Ashfold, M. J., Latif, M. T., Samah, A. A., Mead, M. I., and Harris, N. R. P.: Influence of Northeast Monsoon cold surges on air quality in Southeast Asia, *Atmos. Environ.*, 166, 498–509, <https://doi.org/10.1016/j.atmosenv.2017.07.047>, 2017.
- Behrenfeld, M. J., O'Malley, R. T., Siegel, D. A., McClain, C. R., Sarmiento, J. L., Feldman, G. C., Milligan, A. J., Falkowski, P. G., Letelier, R. M., and Boss, E. S.: Climate-driven trends in contemporary ocean productivity, *Nature*, 444, 752–755, <https://doi.org/10.1038/nature05317>, 2006.
- Bloss, W. J., Evans, M. J., Lee, J. D., Sommariva, R., Heard, D. E., and Pilling, M. J.: The oxidative capacity of the troposphere: Coupling of field measurements of OH and a global chemistry transport model, *Faraday Discuss.*, 130, 425–436, <https://doi.org/10.1039/b419090d>, 2005.
- Boreddy, S. K. R. and Kawamura, K.: A 12-year observation of water-soluble ions in TSP aerosols collected at a remote marine location in the western North Pacific: an outflow region of Asian dust, *Atmos. Chem. Phys.*, 15, 6437–6453, <https://doi.org/10.5194/acp-15-6437-2015>, 2015.
- Boreddy, S. K. R., Kawamura, K., and Jung, J. S.: Hygroscopic properties of particles nebulized from water extracts of aerosols collected at Chichijima Island in the western North Pacific: An outflow region of Asian dust, *J. Geophys. Res.-Atmos.*, 119, 167–178, <https://doi.org/10.1002/2013JD020626>, 2014.
- Bowen, H. J. M.: Environmental chemistry of the elements, Academic Press, London, 1979.
- Carlton, A. G., Turpin, B. J., Lim, H. J., Altieri, K. E., and Seitzinger, S.: Link between isoprene and secondary organic aerosol (SOA): Pyruvic acid oxidation yields low volatility organic acids in clouds, *Geophys. Res. Lett.*, 33, L06822, <https://doi.org/10.1029/2005gl025374>, 2006.
- Carpenter, L. J., Fleming, Z. L., Read, K. A., Lee, J. D., Moller, S. J., Hopkins, J. R., Purvis, R. M., Lewis, A. C., Muller, K., Heinold, B., Herrmann, H., Fomba, K. W., van Pinxteren, D., Muller, C., Tegen, I., Wiedensohler, A., Muller, T., Niedermeier, N., Achterberg, E. P., Patey, M. D., Kozlova, E. A., Heimann, M., Heard, D. E., Plane, J. M. C., Mahajan, A., Oetjen, H., Ingham, T., Stone, D., Whalley, L. K., Evans, M. J., Pilling, M. J., Leigh, R. J., Monks, P. S., Karunaharan, A., Vaughan, S., Arnold, S. R., Tschritter, J., Pöhler, D., Friess, U., Holla, R., Mendes, L. M., Lopez, H., Faria, B., Manning, A. J., and Wallace, D. W. R.: Seasonal characteristics of tropical marine boundary layer air measured at the Cape Verde Atmospheric Observatory, *J. Atmos. Chem.*, 67, 87–140, <https://doi.org/10.1007/s10874-011-9206-1>, 2010.
- Carslaw, D. C.: The openair manual – open-source tools for analysing air pollution data, Manual for version 1.1-4., King's College London, 2015.
- Carslaw, D. C. and Ropkins, K.: openair – An R package for air quality data analysis, *Environ. Modell. Softw.*, 27–28, 52–61, <https://doi.org/10.1016/j.envsoft.2011.09.008>, 2012.
- Charlson, R. J., Langner, J., Rodhe, H., Leovy, C. B., and Warren, S. G.: Perturbation of the Northern-Hemisphere Radiative Balance by Backscattering from Anthropogenic Sulfate Aerosols, *Tellus A*, 43, 152–163, <https://doi.org/10.1034/j.1600-0870.1991.00013.x>, 1991.
- Dominick, D., Latif, M. T., Juneng, L., Khan, M. F., Amil, N., Mead, M. I., Nadzir, M. S. M., Moi, P. S., Abu Samah, A., Ashfold, M. J., Sturges, W. T., Harris, N. R. P., Robinson, A. D., and Pyle, J. A.: Characterisation of particle mass and number concentration on the east coast of the Malaysian Peninsula during the northeast monsoon, *Atmos. Environ.*, 117, 187–199, <https://doi.org/10.1016/j.atmosenv.2015.07.018>, 2015.
- Draxler, R. R. and Hess, G. D.: Description of the HYSPLIT\_4 modeling system, NOAA Air Resources Laboratory, Silver Spring, MD, NOAA Tech. Memo. ERL ARL-224, 24, 1997.
- Draxler, R. R. and Hess, G. D.: An overview of the HYSPLIT\_4 modeling system of trajectories, dispersion, and deposition, *Aust. Meteorol. Mag.*, 47, 295–308, 1998.
- Draxler, R. R.: HYSPLIT4 user's guide, NOAA Air Resources Laboratory, Silver Spring, MD, NOAA Tech. Memo. ERL ARL-230, 1999.
- Dunmore, R. E., Hopkins, J. R., Lidster, R. T., Mead, M. I., Bandy, B. J., Forster, G., Oram, D. E., Sturges, W. T., Phang, S. M., Abu Samah, A., and Hamilton, J. F.: Development of a Combined Heart-Cut and Comprehensive Two-Dimensional Gas Chromatography System to Extend the Carbon Range of Volatile Organic Compounds Analysis in a Single Instrument, *Separations*, 3, 21, <https://doi.org/10.3390/separations3030021>, 2016.
- EPA: 40 Protection of Environment Part 136 Guidelines Establishing Test Procedures for the Analysis of Pollutants, in: Electronic Code of Federal Regulations, U.S. Government Publishing Office, Washington, DC, available at: [https://www.ecfr.gov/cgi-bin/text-idx?SID=57d5771415f8a36cb8c0e2ca2a1583a2&mc=true&node=pt40.25.136&rgn=div5#ap40.25.136\\_17.b](https://www.ecfr.gov/cgi-bin/text-idx?SID=57d5771415f8a36cb8c0e2ca2a1583a2&mc=true&node=pt40.25.136&rgn=div5#ap40.25.136_17.b), last access: 20 July 2017.
- Facchini, M. C., Mircea, M., Fuzzi, S., and Charlson, R. J.: Cloud albedo enhancement by surface-active organic solutes in growing droplets, *Nature*, 401, 257–259, <https://doi.org/10.1038/45758>, 1999.
- Farren, N. J., Dunmore, R. E., Mead, M. I., Mohd Nadzir, M. S., Samah, A. A., Phang, S.-M., Bandy, B. J., Sturges, W. T., and Hamilton, J. F.: Chemical Characterisation of Water-soluble Ions in Atmospheric Particulate Matter on the East Coast of Peninsular Malaysia, <https://doi.org/10.15124/bd4a9045-832b-4ff8-aecc-ef1653603f1d>, 2018.
- Fisher, J. A., Jacob, D. J., Wang, Q. Q., Bahreini, R., Carouge, C. C., Cubison, M. J., Dibb, J. E., Diehl, T., Jimenez, J. L., Leibensperger, E. M., Lu, Z. F., Meinders, M. B. J., Pye, H. O. T., Quinn, P. K., Sharma, S., Streets, D. G., van Donkelaar, A., and Yantosca, R. M.: Sources, distribution, and acidity of sulfate-ammonium aerosol in the Arctic in winter-spring, *Atmos. Environ.*, 45, 7301–7318, <https://doi.org/10.1016/j.atmosenv.2011.08.030>, 2011.
- Fountoukis, C. and Nenes, A.: ISORROPIA II: a computationally efficient thermodynamic equilibrium model for  $K^+$ - $Ca^{2+}$ - $Mg^{2+}$ - $NH_4^+$ - $Na^+$ - $SO_4^{2-}$ - $NO_3^-$ - $Cl^-$ - $H_2O$  aerosols, *Atmos. Chem. Phys.*, 7, 4639–4659, <https://doi.org/10.5194/acp-7-4639-2007>, 2007.
- Freitas, A. D., Martins, L. D., and Solci, M. C.: Size-Segregated Particulate Matter and Carboxylic Acids over Urban and Rural Sites in Londrina City, Brazil, *J. Brazil Chem. Soc.*, 23, 921–930, 2012.
- Garreaud, R. D.: Subtropical cold surges: Regional aspects and global distribution, *Int. J. Climatol.*, 21, 1181–1197, <https://doi.org/10.1002/Joc.687>, 2001.

- GAW-SIS (Global Atmospheric Watch Station Information System): available at: <https://gawsis.meteoswiss.ch/GAWISIS/index.html#/>, last access: 12 April 2017.
- Giglio, L., Descloitres, J., Justice, C. O., and Kaufman, Y. J.: An enhanced contextual fire detection algorithm for MODIS, *Remote Sens. Environ.*, **87**, 273–282, [https://doi.org/10.1016/S0034-4257\(03\)00184-6](https://doi.org/10.1016/S0034-4257(03)00184-6), 2003.
- Ginoux, P., Prospero, J. M., Gill, T. E., Hsu, N. C., and Zhao, M.: Global-Scale Attribution of Anthropogenic and Natural Dust Sources and Their Emission Rates Based on Modis Deep Blue Aerosol Products, *Rev. Geophys.*, **50**, RG3005, <https://doi.org/10.1029/2012rg000388>, 2012.
- Gwynn, R. C., Burnett, R. T., and Thurston, G. D.: A time-series analysis of acidic particulate matter and daily mortality and morbidity in the Buffalo, New York, region, *Environ. Health Persp.*, **108**, 125–133, <https://doi.org/10.2307/3454510>, 2000.
- Hennigan, C. J., Izumi, J., Sullivan, A. P., Weber, R. J., and Nenes, A.: A critical evaluation of proxy methods used to estimate the acidity of atmospheric particles, *Atmos. Chem. Phys.*, **15**, 2775–2790, <https://doi.org/10.5194/acp-15-2775-2015>, 2015.
- Huang, X. F. and Yu, J. Z.: Is vehicle exhaust a significant primary source of oxalic acid in ambient aerosols?, *Geophys. Res. Lett.*, **34**, L02808, <https://doi.org/10.1029/2006gl028457>, 2007.
- Huang, X. F., Yu, J. Z., He, L. Y., and Yuan, Z. B.: Water-soluble organic carbon and oxalate in aerosols at a coastal urban site in China: Size distribution characteristics, sources, and formation mechanisms, *J. Geophys. Res.-Atmos.*, **111**, D22212, <https://doi.org/10.1029/2006jd007408>, 2006.
- Ismail, M., Yuen, F. S., and Abdullah, S. S.: Particulate Matter Status and its Relationship with Meteorological Factors in the East Coast of Peninsular Malaysia, *J. Eng. Appl. Sci.*, **11**, 2588–2593, 2016.
- Jiang, Y., Zhuang, G., Wang, Q., Liu, T., Huang, K., Fu, J. S., Li, J., Lin, Y., Zhang, R., and Deng, C.: Characteristics, sources and formation of aerosol oxalate in an Eastern Asia megacity and its implication to haze pollution, *Atmos. Chem. Phys. Discuss.*, **11**, 22075–22112, <https://doi.org/10.5194/acpd-11-22075-2011>, 2011.
- Kerminen, V. M.: Relative roles of secondary sulfate and organics in atmospheric cloud condensation nuclei production, *J. Geophys. Res.-Atmos.*, **106**, 17321–17333, <https://doi.org/10.1029/2001jd900204>, 2001.
- Keywood, M. D., Ayers, G. P., Gras, J. L., Boers, C. P., and Leong: Haze in the Klang Valley of Malaysia, *Atmos. Chem. Phys.*, **3**, 591–605, <https://doi.org/10.5194/acp-3-591-2003>, 2003.
- Lawrence, M. G., Jöckel, P., and von Kuhlmann, R.: What does the global mean OH concentration tell us?, *Atmos. Chem. Phys.*, **1**, 37–49, <https://doi.org/10.5194/acp-1-37-2001>, 2001.
- Legrand, M. and Pasteur, E. C.: Methane sulfonic acid to non-sea-salt sulfate ratio in coastal Antarctic aerosol and surface snow, *J. Geophys. Res.-Atmos.*, **103**, 10991–11006, <https://doi.org/10.1029/98jd00929>, 1998.
- Lin, Y. H., Zhang, Z. F., Docherty, K. S., Zhang, H. F., Budisulistiorini, S. H., Rubitschun, C. L., Shaw, S. L., Knipping, E. M., Edgerton, E. S., Kleindienst, T. E., Gold, A., and Surratt, J. D.: Isoprene Epoxydiols as Precursors to Secondary Organic Aerosol Formation: Acid-Catalyzed Reactive Uptake Studies with Authentic Compounds, *Environ. Sci. Technol.*, **46**, 250–258, <https://doi.org/10.1021/es202554c>, 2012.
- Murphy, J. G., Gregoire, P. K., Tevlin, A. G., Wentworth, G. R., Ellis, R. A., Markovic, M. Z., and Vandenboer, T. C.: Observational constraints on particle acidity using measurements and modelling of particles and gases, *Faraday Discuss.*, **200**, 379–395, 2017.
- Myriokefalitakis, S., Tsigaridis, K., Mihalopoulos, N., Sciare, J., Nenes, A., Kawamura, K., Segers, A., and Kanakidou, M.: In-cloud oxalate formation in the global troposphere: a 3-D modeling study, *Atmos. Chem. Phys.*, **11**, 5761–5782, <https://doi.org/10.5194/acp-11-5761-2011>, 2011.
- Neale, R. and Slingo, J.: The maritime continent and its role in the global climate: A GCM study, *J. Climate*, **16**, 834–848, [https://doi.org/10.1175/1520-0442\(2003\)016<0834:Tmcair>2.0.Co;2](https://doi.org/10.1175/1520-0442(2003)016<0834:Tmcair>2.0.Co;2), 2003.
- Newberg, J. T., Matthew, B. M., and Anastasio, C.: Chloride and bromide depletions in sea-salt particles over the north-eastern Pacific Ocean, *J. Geophys. Res.-Atmos.*, **110**, D06209, <https://doi.org/10.1029/2004jd005446>, 2005.
- NOAA (National Oceanic and Atmospheric Administration Integrated Surface Database): available at: <https://www.ncdc.noaa.gov/isd> (last access: 20 July 2017), 2003.
- Novakov, T. and Penner, J. E.: Large Contribution of Organic Aerosols to Cloud-Condensation-Nuclei Concentrations, *Nature*, **365**, 823–826, <https://doi.org/10.1038/365823a0>, 1993.
- Oram, D. E., Ashfold, M. J., Laube, J. C., Gooch, L. J., Humphrey, S., Sturges, W. T., Leedham-Elvidge, E., Forster, G. L., Harris, N. R. P., Mead, M. I., Samah, A. A., Phang, S. M., Ou-Yang, C.-F., Lin, N.-H., Wang, J.-L., Baker, A. K., Brenninkmeijer, C. A. M., and Sherry, D.: A growing threat to the ozone layer from short-lived anthropogenic chlorocarbons, *Atmos. Chem. Phys.*, **17**, 11929–11941, <https://doi.org/10.5194/acp-17-11929-2017>, 2017.
- Pyle, J. A., Ashfold, M. J., Harris, N. R. P., Robinson, A. D., Warwick, N. J., Carver, G. D., Gostlow, B., O'Brien, L. M., Manning, A. J., Phang, S. M., Yong, S. E., Leong, K. P., Ung, E. H., and Ong, S.: Bromoform in the tropical boundary layer of the Maritime Continent during OP3, *Atmos. Chem. Phys.*, **11**, 529–542, <https://doi.org/10.5194/acp-11-529-2011>, 2011.
- Ripp, J.: Analytical Detection Limit Guidance and Laboratory Guide for Determining Method Detection Limits, Wisconsin Department of Natural Resources, Madison, WI, PUBL-TS-056-96, 1996.
- Robinson, A. D., Harris, N. R. P., Ashfold, M. J., Gostlow, B., Warwick, N. J., O'Brien, L. M., Beardmore, E. J., Nadzir, M. S. M., Phang, S. M., Samah, A. A., Ong, S., Ung, H. E., Peng, L. K., Yong, S. E., Mohamad, M., and Pyle, J. A.: Long-term halocarbon observations from a coastal and an inland site in Sabah, Malaysian Borneo, *Atmos. Chem. Phys.*, **14**, 8369–8388, <https://doi.org/10.5194/acp-14-8369-2014>, 2014.
- Sareen, N., Carlton, A. G., Surratt, J. D., Gold, A., Lee, B., Lopez-Hilfiker, F. D., Mohr, C., Thornton, J. A., Zhang, Z., Lim, Y. B., and Turpin, B. J.: Identifying precursors and aqueous organic aerosol formation pathways during the SOAS campaign, *Atmos. Chem. Phys.*, **16**, 14409–14420, <https://doi.org/10.5194/acp-16-14409-2016>, 2016.
- Savoie, D. L. and Prospero, J. M.: Comparison of Oceanic and Continental Sources of Non-Sea-Salt Sulfate over the Pacific-Ocean, *Nature*, **339**, 685–687, <https://doi.org/10.1038/339685a0>, 1989.



- Saxena, P. and Hildemann, L. M.: Water-soluble organics in atmospheric particles: A critical review of the literature and application of thermodynamics to identify candidate compounds, *J. Atmos. Chem.*, 24, 57–109, <https://doi.org/10.1007/Bf00053823>, 1996.
- Seinfeld, J. H. and Pandis, S. N.: Atmospheric chemistry and physics: from air pollution to climate change, 1–1203, 2nd Edn., J. Wiley, Hoboken, NJ, 2006.
- Sempere, R. and Kawamura, K.: Comparative Distributions of Dicarboxylic-Acids and Related Polar Compounds in Snow Rain and Aerosols from Urban Atmosphere, *Atmos. Environ.*, 28, 449–459, [https://doi.org/10.1016/1352-2310\(94\)90123-6](https://doi.org/10.1016/1352-2310(94)90123-6), 1994.
- Stein, A. F., Draxler, R. R., Rolph, G. D., Stunder, B. J. B., Cohen, M. D., and Ngan, F.: NOAA's Hysplit Atmospheric Transport and Dispersion Modeling System, *B. Am. Meteorol. Soc.*, 96, 2059–2077, <https://doi.org/10.1175/Bams-D-14-00110.1>, 2015.
- Sturges, W. T. and Shaw, G. E.: Halogens in Aerosols in Central Alaska, *Atmos. Environ. A-Gen.*, 27, 2969–2977, [https://doi.org/10.1016/0960-1686\(93\)90329-W](https://doi.org/10.1016/0960-1686(93)90329-W), 1993.
- Surratt, J. D., Chan, A. W. H., Eddingsaas, N. C., Chan, M. N., Loza, C. L., Kwan, A. J., Hersey, S. P., Flagan, R. C., Wennberg, P. O., and Seinfeld, J. H.: Reactive intermediates revealed in secondary organic aerosol formation from isoprene, *P. Natl. Acad. Sci. USA*, 107, 6640–6645, <https://doi.org/10.1073/pnas.0911114107>, 2010.
- Tahir, N. M., Suratman, S., Fong, F. T., Hamzah, M. S., and Latif, M. T.: Temporal Distribution and Chemical Characterization of Atmospheric Particulate Matter in the Eastern Coast of Peninsular Malaysia, *Aerosol Air Qual. Res.*, 13, 584–595, <https://doi.org/10.4209/aaqr.2012.08.0216>, 2013.
- Tan, Y., Lim, Y. B., Altieri, K. E., Seitzinger, S. P., and Turpin, B. J.: Mechanisms leading to oligomers and SOA through aqueous photooxidation: insights from OH radical oxidation of acetic acid and methylglyoxal, *Atmos. Chem. Phys.*, 12, 801–813, <https://doi.org/10.5194/acp-12-801-2012>, 2012.
- Yamasoe, M. A., Artaxo, P., Miguel, A. H., and Allen, A. G.: Chemical composition of aerosol particles from direct emissions of vegetation fires in the Amazon Basin: water-soluble species and trace elements, *Atmos. Environ.*, 34, 1641–1653, [https://doi.org/10.1016/S1352-2310\(99\)00329-5](https://doi.org/10.1016/S1352-2310(99)00329-5), 2000.
- Zhang, Y., Sperber, K. R., and Boyle, J. S.: Climatology and interannual variation of the East Asian winter monsoon: Results from the 1979–95 NCEP/NCAR reanalysis, *Mon. Weather Rev.*, 125, 2605–2619, [https://doi.org/10.1175/1520-0493\(1997\)125<2605:Caivot>2.0.Co;2](https://doi.org/10.1175/1520-0493(1997)125<2605:Caivot>2.0.Co;2), 1997.